Supporting Information:

Materials

PBDB-T-2F, PBDB-TF or PM6: poly[(2,6-(4,8-bis(5-(2-ethylhexyl-3-fluoro)thiophen-2-yl)-benzo[1,2-b:4,5-b’]dithiophene))-alt-(5,5-(1’,3’-di-2-thienyl-5’,7’-bis(2-ethylhexyl)benzo[1’,2’-c:4’,5’-c’]dithiophene-4,8-dione)].

eC9: 2,2'- [[12,13-Bis(2-butyloctyl)-12,13-dihydro-3,9-dinonylbisthieno[2",3":4',5']thieno[2',3':4,5]pyrrolo[3,2-e:2',3'-g][2,1,3]benzothiadiazole-2,10-diyl]bis[methylidyne(5,6-chloro-3-oxo-1H-indene-2,1(3H)-diylidene)]]bis[propanedinitrile]

L8-BO: 2,2'-((2Z,2'Z)-((12,13-bis(2-ethylhexyl)-3,9-(2-butyloctyl)-12,13-dihydro-[1,2,5]thiadiazolo[3,4-e]thieno[2",3’':4’,5']thieno[2',3':4,5]pyrrolo[3,2-g]thieno[2',3':4,5]thieno[3,2-b]indole-2,10-diyl)bis(methanylylidene))bis(5,6-difluoro-3-oxo-2,3-dihydro-1H-indene-2,1-diylidene))dimalononitrile

PFN-Br: Poly(9,9-bis(3’-(N,N-dimethyl)-N-ethylammoinium-propyl-2,7-fluorene)-alt-2,7-(9,9-dioctylfluorene))dibromide

All above materials are purchased from Solarmer Inc.

MA: melamine

PFN-Br-MA: doped PFN-Br by MA instructed by ref 46 in the main text.

Chloroform, chlorobenzene and ortho-xylene are from Sigma-Aldrich Inc.

PEDOT:PSS with the type of Clevios P VP AI 4083 was obtain from Heraeus.

The leaser patterned ITO substrates (15 Ω cm^{-2}) were purchased from were obtained from South China Xiang City Inc.

All reagents and solids were used as received without any further purification.

Characterization

UV-vis absorption spectra were measured using a Shimadzu UV-2500 recording spectrophotometer. TEM was recorded on a JEOL JEM-2100 operated at 120kV. The grazing incidence small/wide angle X-ray scattering (GISAXS/GIWAXS) measurements were carried out with a Ganesha SAXSLAB laboratory instrument using a CuKα X-ray source (8.05 keV, 1.54 Å) and a Pilatus 300K detector. The samples for GIWAXS/GISAXS measurements were fabricated on silicon substrates using the same recipe as for the devices. The incident angle was 0.4° for GISAXS and 0.2° for GIWAXS measurements, respectively. The sample to detector distance (SDD) was set to 1045 and 95 mm for GISAXS and GIWAXS measurement. For the GISAXS images, the DPDAK software was applied to extract the polymer scattering signals. The transformation to q-space, radial cuts for the in-plane and out-of-plane analysis and azimuthal cuts for the orientation analysis were processed by the MATLAB-based package GIXSGUI. Contact angle tests were achieved by an Attension Theta Flex meter.

Solar cell fabrication and characterization

Solar cells were fabricated in a conventional device configuration of ITO/PEDOT:PSS-TA/active layers/PFN-Br-MA/Ag. The ITO substrates (~94% transmittance) were first scrubbed by detergent and then sonicated with deionized water, acetone and isopropanol subsequently, and dried overnight in an oven. The glass substrates were treated by UV-Ozone for 30 min before use. PEDOT:PSS-TA (1mg/ml tyramine doped in standard Hareus Al 4083 solution) was spin-cast onto the ITO substrates at 7500 rpm for 30 s, and then dried at 160 °C for 15 min in air. The blend of PM6:acceptor (eC9 or L8-BO) (1:1.2 in weight) blends were dissolved in CF (7 mg mL^{-1} donor concentration), CB (10 mg mL^{-1} donor concentration), and XY (11 mg mL^{-1} donor concentration), with DIO (0.25% vol) as additive, and stirred on a 80 °C hotplate for 2 hours a nitrogen-filled glove box. The blend solution was spin-cast at 2000 rpm for 50 s onto PEDOT:PSS-TA films followed by a temperature anealing of 100°C for 1 min. PFN-Br-MA (melamine doped with 0.25% weight ratio) thin layers were coated on the active layer with 3000 rpm (0.5 mg mL^{-1}), followed by the deposition of Ag (150 nm) (evaporated under 1×10^{-3} Pa through a shadow mask). The optimal active layer thickness measured by a Bruker Dektak XT stylus profilometer was about 105 nm. The current density-voltage (J-V) curves of devices were measured using a Keysight B2901A Source Meter in glove box under AM 1.5G (100 mW cm^{-2}) using a Enlitech solar simulator. The device contact area was 0.05 cm^2, device illuminated area during testing was 0.04 cm2, which was determined by a mask. The EQE spectra were measured using a Solar Cell Spectral Response Measurement System QE-R3011 (Enlitech Co., Ltd.). The light intensity at each wavelength was calibrated using a standard monocrystalline Si photovoltaic cell.

Open-air Blade Coating for Active Layers

The blade coat films were fabricated by XY solutions (11 mg mL^{-1} donor concentration, for binary and ternary blends; 80°C to ensure materials are fully dissolved.) with a 20 mm/s speed forward and backward (the blade-substrate gap is c.a. 120 μm) on room temperature ITO/PEDOT:PSS substrates, and then transferred (after c.a. 15 s) to a nearby hotplate to be annealed at a100°C hotplate for 1 min. These steps are all carried out in ambient atmosphere with a 50% RH humidity. The N_2 knife is used to properly accelerating the film drying, to make the blade coated film has a similar drying kinetics as spin coated counterparts does, and prevent any unexpected morphology destruction caused by too slow evaporation. The knife is achieved by gas pipeline releasing N_2 with controllable intensity and direction (normally parallel to the film).

SCLC Measurements

The electron and hole mobility were measured by using the method of space-charge limited current (SCLC) for electron-only devices with the structure of ITO/ZnO/active layer/PFN-Br-MA/Ag and hole-only devices with the structure of ITO/PEDOT:PSS-TA/active layers/MoO_x/Ag. The charge carrier mobility was determined by fitting the dark current to the model of a single carrier SCLC according to the equation: $J = 9\varepsilon_0\varepsilon_r\mu V^2/8d^3$, where J is the current density, d is the film thickness of the active layer, μ is the charge carrier mobility, ε_r is the relative dielectric constant of the transport medium, and ε_0 is the permittivity of free space. $V = V_{app} - V_{bi}$, where V_{app} is the applied voltage, V_{bi} is the offset voltage. The charge carrier mobility was calculated from the slope of the $J^{1/2} \sim V$ curves. The thickness of target layer is well controlled identical to that of PV's active layer. The SCLC region for mobility fitting is determined by a recent literature's (*Nat. Mater.*, 2022, **21**, 656-663) method.

Surface Tension Characterization

Contact angle measurements were carried out by an Attension Theta Flex meter, using water and ethylene glycol by sessile drop analysis.

The surface tension values of films were calculated by the Wu method, in which:

$$\gamma_{Water}(cos\theta_{Water} + 1) = \frac{4\gamma_{water}^{d}\cdot\gamma^{d}}{\gamma_{water}^{d} + \gamma^{d}} + \frac{4\gamma_{water}^{p}\cdot\gamma^{p}}{\gamma_{water}^{p} + \gamma^{p}}$$

$$\gamma_{EG}(cos\theta_{EG} + 1) = \frac{4\gamma_{EG}^{d}\cdot\gamma^{d}}{\gamma_{EG}^{d} + \gamma^{d}} + \frac{4\gamma_{EG}^{p}\cdot\gamma^{p}}{\gamma_{EG}^{p} + \gamma^{p}}$$

$$\gamma = \gamma^{d} + \gamma^{p}$$

where θ is the contact angle of each thin film, and γ is the surface free energy of samples, which is equal to the sum of the dispersion (γ^{d}) and polarity (γ^{p}) components; γ_{water} and γ_{EG} are the surface tensions of the water and ethylene glycol; and γ_{water}^{d}, γ_{water}^{p}, γ_{EG}^{d} and γ_{EG}^{p} are the dispersion and polarity components of γ_{Water} and γ_{EG}.

While the OWRK model is done by:

$$\gamma_{L}(cos\theta + 1) = 2\ ((\gamma_{S}^{d}\cdot\gamma_{L}^{d}){}^\wedge 0.5 + ((\gamma_{S}^{p}\cdot\gamma_{L}^{p}){}^\wedge 0.5)$$

Where θ is the contact angle (°) between solid and liquid, γ_{L}, γ_{L}^{d}, γ_{L}^{p} are the total, dispersive and polar surface free energies of liquid, and γ_{S}^{d}, γ_{S}^{p} are the dispersive and polar components of solid surface free energy, respectively.

The Analysis of J_{ph} vs V_{eff} relationships

The definition of J_{ph} is the current density under illumination (J_{L}) minus the dark current density (J_{D}), and V_{0} refers to the voltage value when $J_{ph} = 0$. Accordingly, $V_{eff} = V_{0} - V_{appl}$, where V_{appl} represents applied voltage, has a clear meaning. Importantly, when V_{eff} reaches a high value (> 2V) it is normally believed that generated excitons are fully collected, in which J_{ph} is equal to saturated current density (J_{sat}). Then, we can calculate J_{SC}/J_{sat} and J_{max}/J_{sat} to describe exciton dissociation (η_{diss}) and charge collection (η_{coll}) efficiency. J_{max} is the J_{ph} at the maximal output point.

FTPS-EQE, EQE$_{EL}$ and EL Characterizations

FTPS-EQE was measured using Vertex 70 from Bruker Optics, equipped with a quartz tungsten halogen lamp, quartz beam splitter and external detector option. A low-noise current amplifier (SR570) was used to amplify the photocurrent produced on illumination of the photovoltaic devices with light modulated by the Fourier transform infrared spectroscope (FTIR). The output voltage of the current amplifier was fed back into the external detector port of the FTIR, to be able to use the FTIR's software to collect the photocurrent spectrum.

EQE$_{EL}$ values were obtained from an in-house-built system including a Hamamatsu silicon photodiode 1010B, a Keithley 2400 SourceMeter to provide voltage and record injected current, and a Keithley 485 Picoammeter to measure the emitted light intensity. EL spectra were measured using a light guide positioned close to the sample. The bias of EL measurement was applied on the devices using a Keithley 2400 Source Meter. The detector was a Newton EM-CCD Si array detector at -60 ºC with a Shamrock SR-303i spectrograph from Andor Tech.

In-situ PL measurements

A custom-designed photoluminescence spectrometer combined with a spin-coater (Novocontrol Tech. GmbH & Co. KG, SCI-10, Germany) was used to perform in-situ PL measurements in ambient conditions. A 405 nm laser diode with a rated power output of 4.5 mW was used as the excitation source. A photodetector (Instrument Systems GmbH, CAS 140 CT, Germany) was used to detect the reflection PL signal simultaneously in a broad variety of wavelengths from 250 nm to 1000 nm with high time resolution (50 ms/spectrum). The information extraction method is simply locating the peak and obtaining corresponding intensity, and integrating the peak area within the FWHM (full width at half maximum) range.

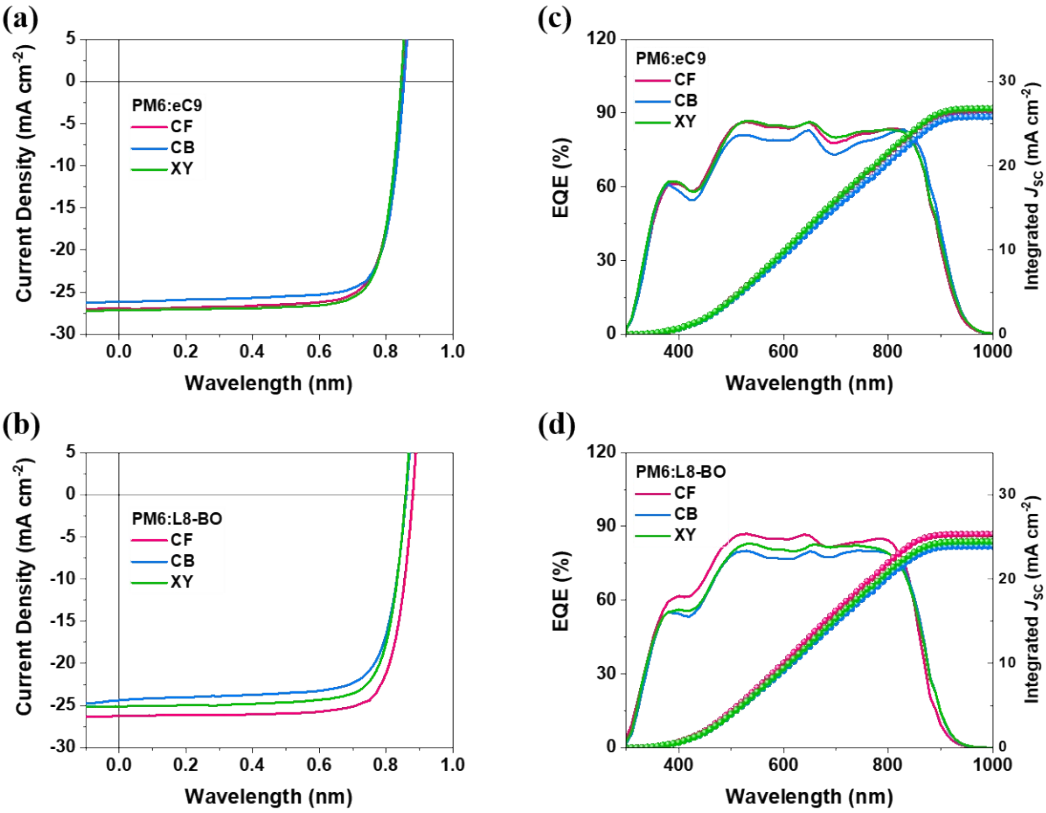

Figure S1. *J-V* characteristics of (a) PM6 eC9 and (b) PM6:L8-BO systems processed from CF, CB and XY. Corresponding EQE spectra of (c) PM6 eC9 and (d) PM6:L8-BO systems.

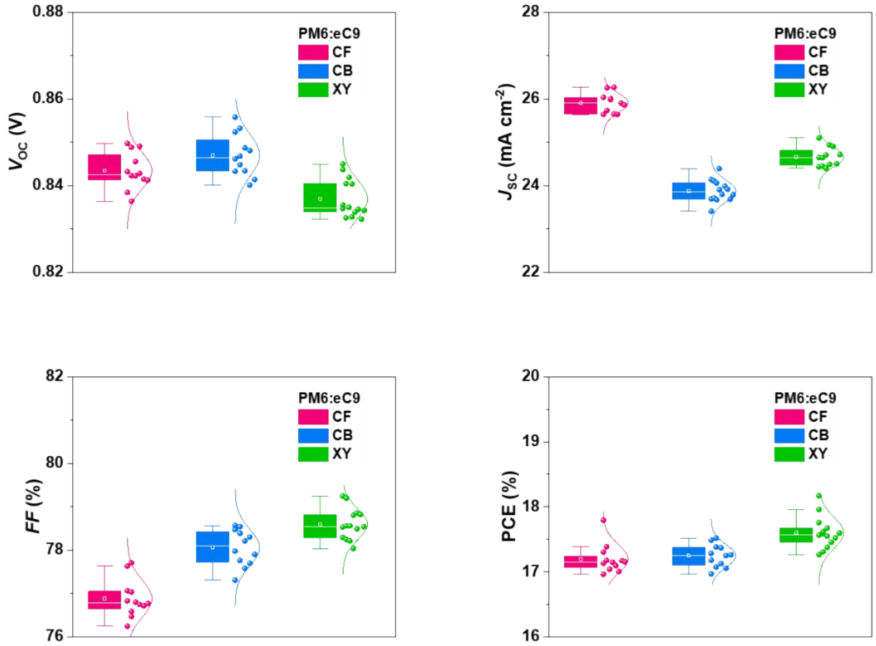

Figure S2. Normal distribution of indenpendent device results for PM6:eC9 system.

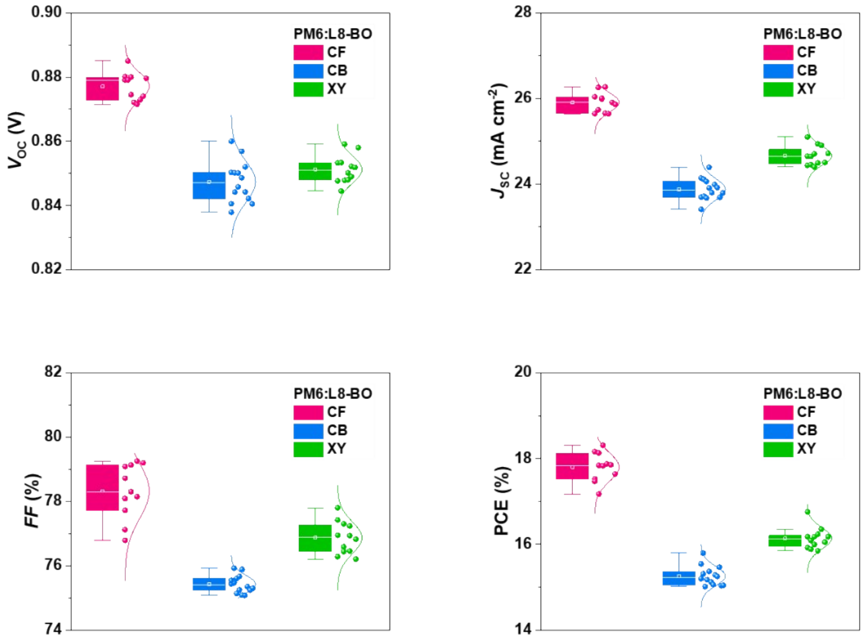

Figure S3. Normal distribution of indenpendent device results for PM6:L8-BO system.

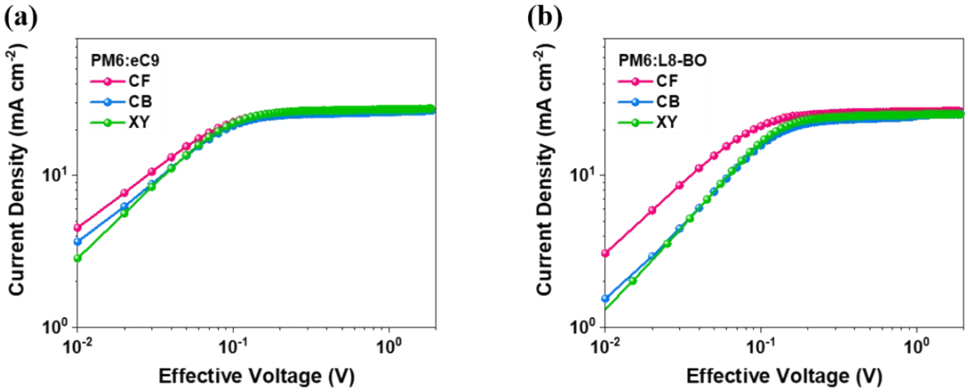

Figure S4. J_{ph} vs V_{eff} relationships of (a) PM6:eC9 and (b) PM6:L8-BO.

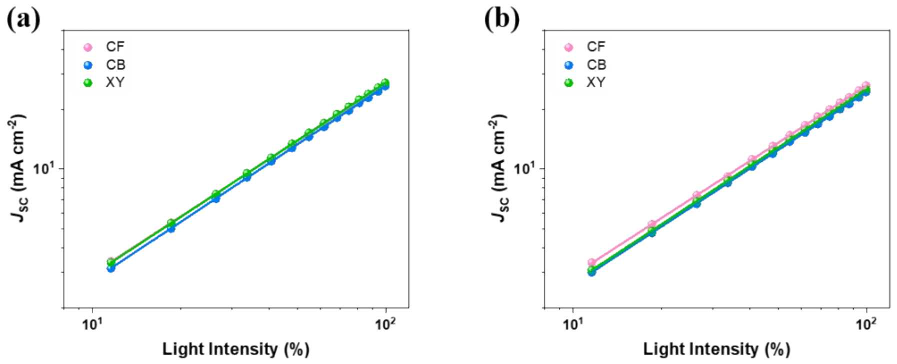

Figure S5. J_{SC} vs P_{light} relationships of (a) PM6:eC9 and (b) PM6:L8-BO solar cells.

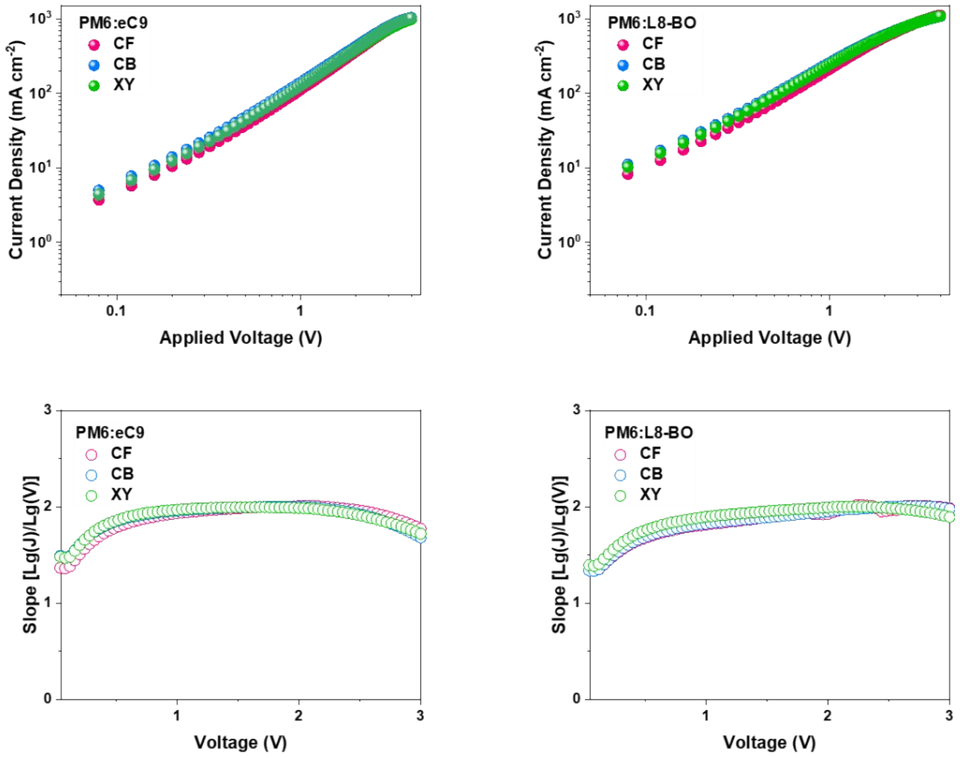

Figure S6.Hole-only device results of PM6:eC9 and PM6-L8-BO blend films in terms of lg*J*-lg*V* and d(lg*J*)/d(lg*V*)-V relationships.

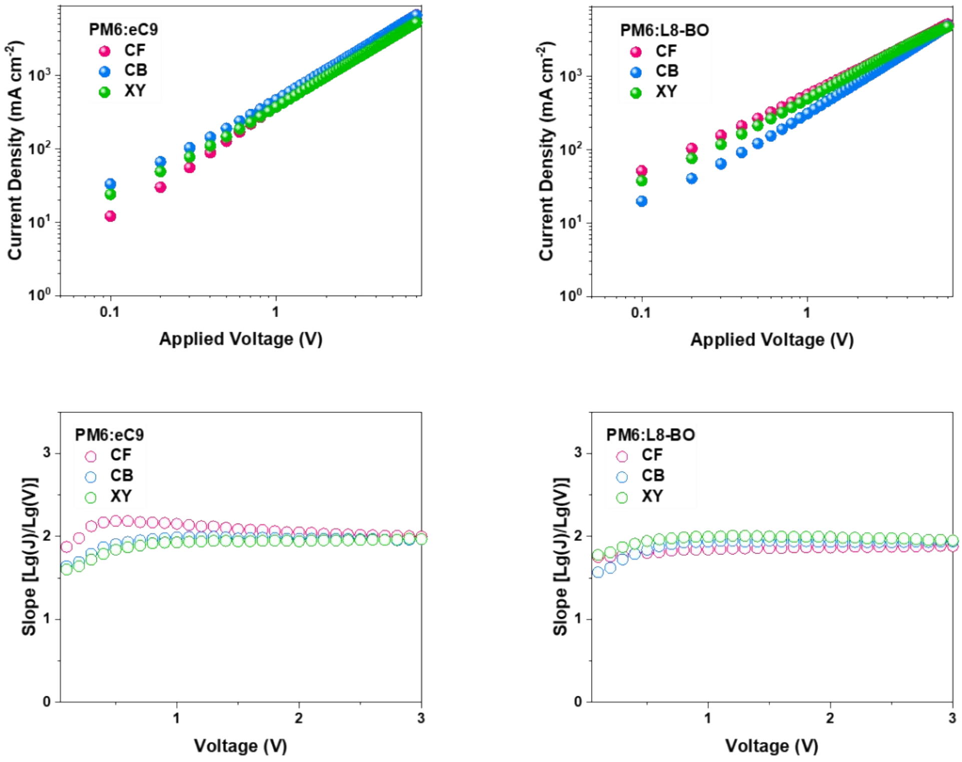

Figure S7.Electron-only device results of PM6:eC9 and PM6-L8-BO blend films.

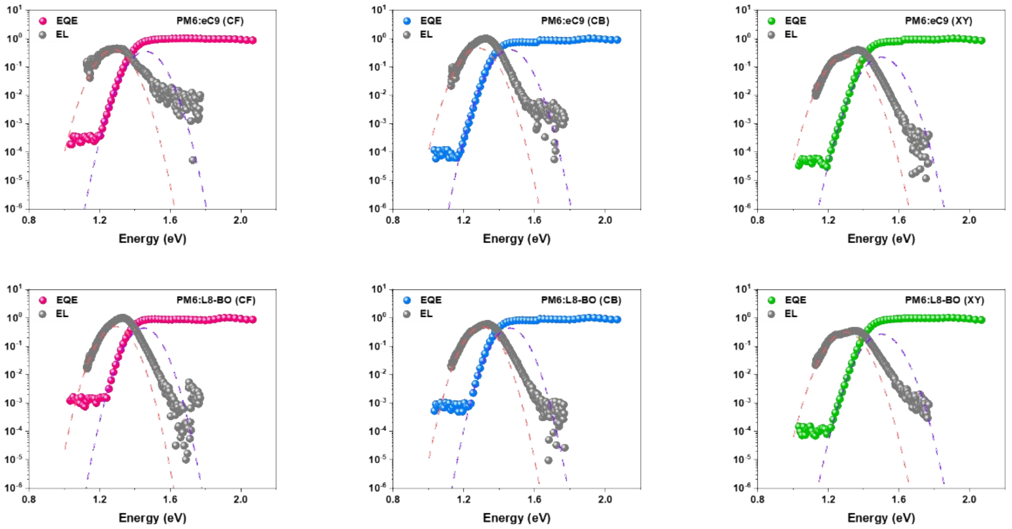

Figure S8.FTPS-EQE + EL spectra of each device and correponding fit lines.

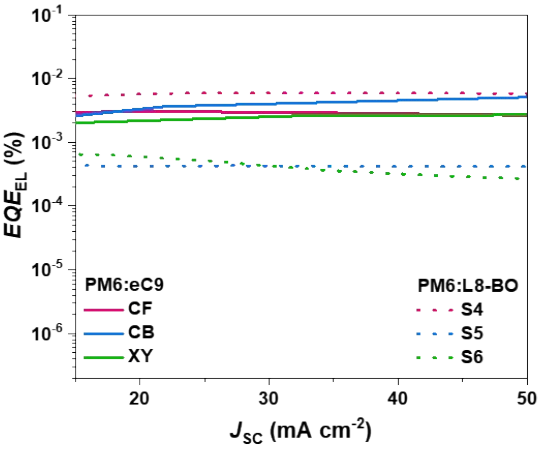

Figure S9.EQE$_{EL}$ of PM6 eC9 and PM6:L8-BO devices.

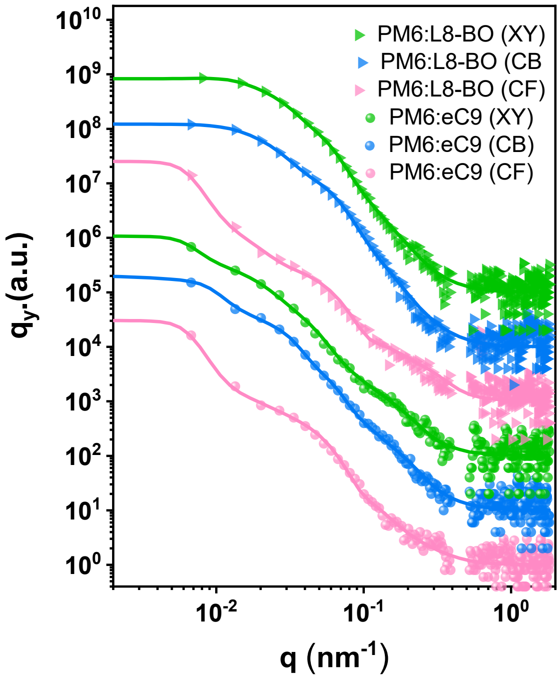

Figure S10. Horizontal line cuts of the 2D GISAXS data for PM6 eC9 and PM6:L8-BO films.

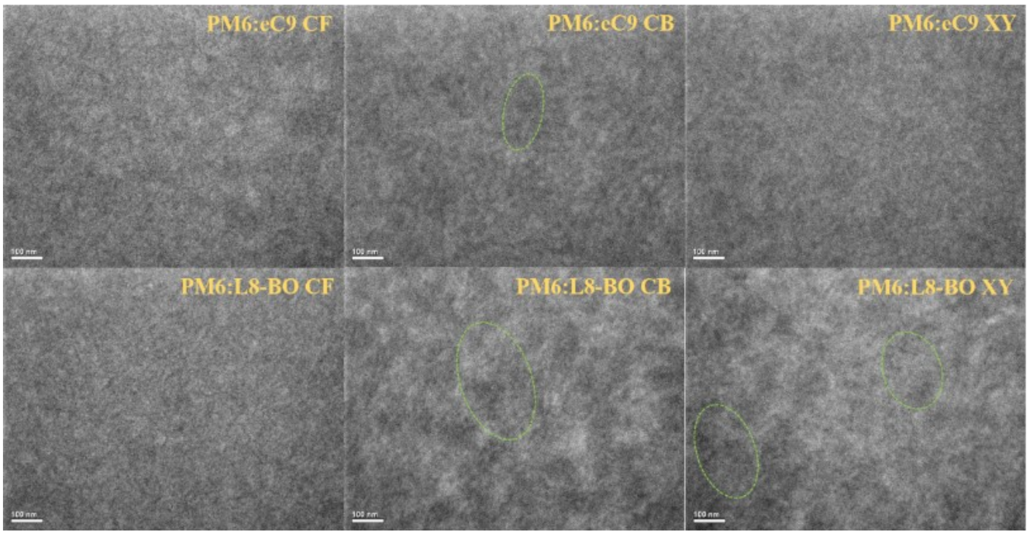

Figure S11. TEM images of active layers with characteristic features highlight by the green dashed circles.

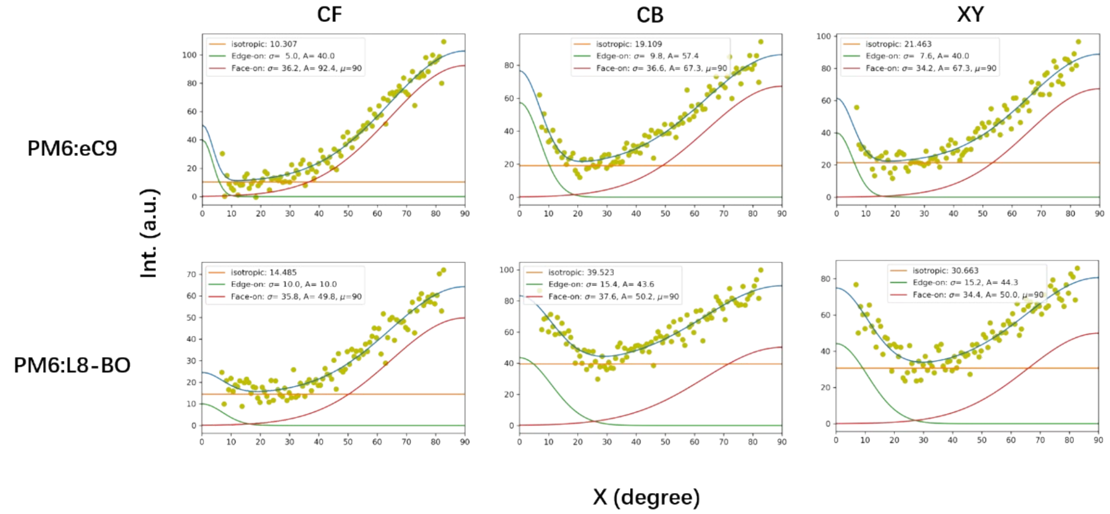

Figure S12. Fit details of tube cuts showing intensity vs. χ performed at the (100) peak in the 2D GIWAXS data.

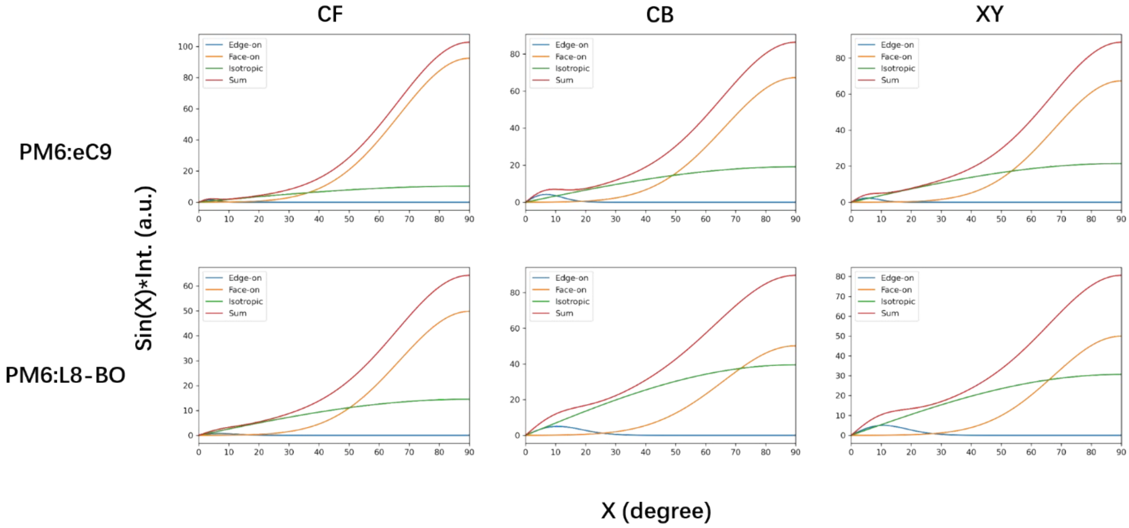

Figure S13. Fit details of tube cuts in the pole figure representation as sin(χ)*intensity vs χ performed at the (100) peak in the 2D GIWAXS data.

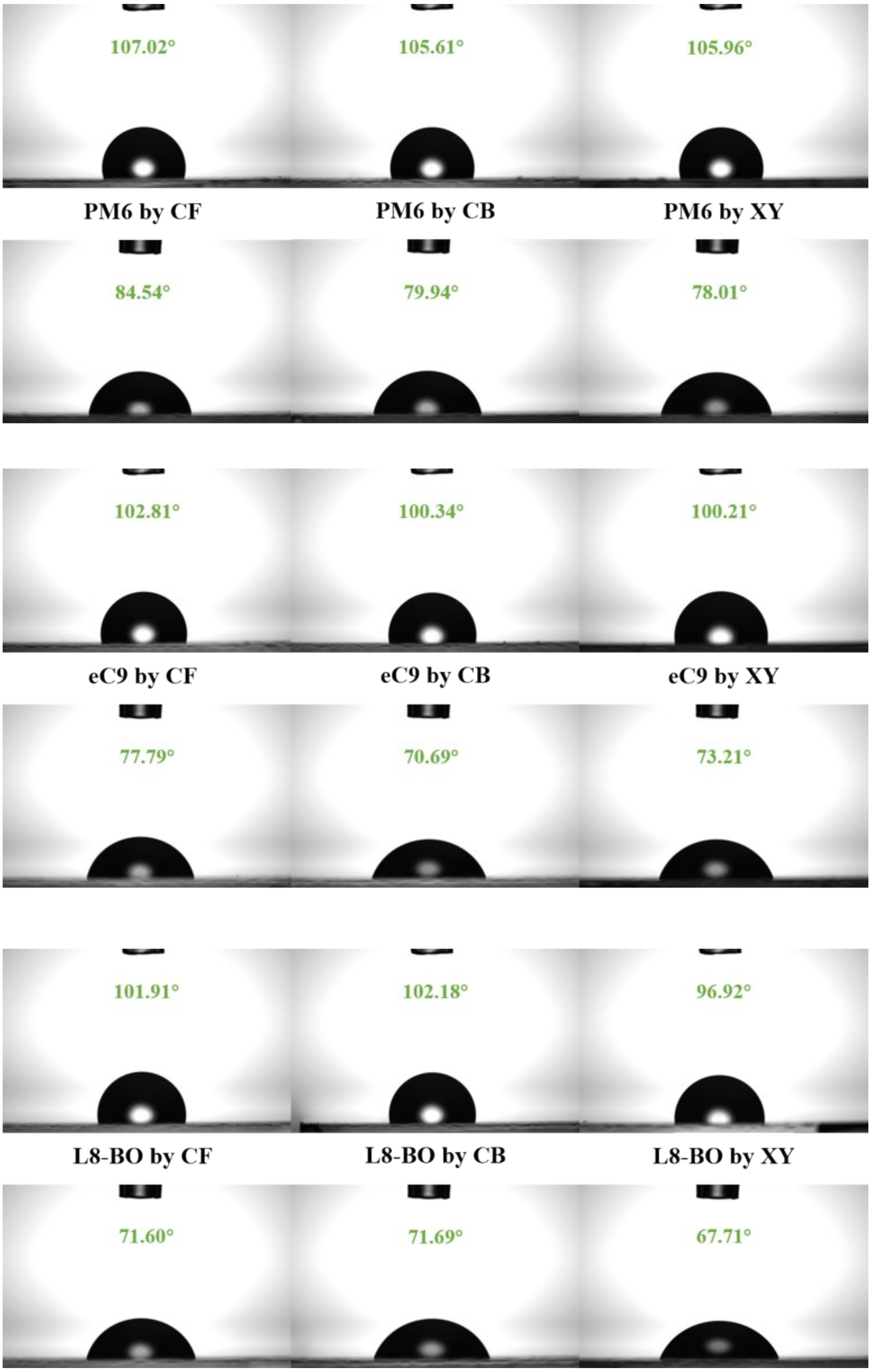

Figure S14. Photographs of the water (upper) and EG (lower) contact angles of PM6, eC9 and L8-BO neat films.

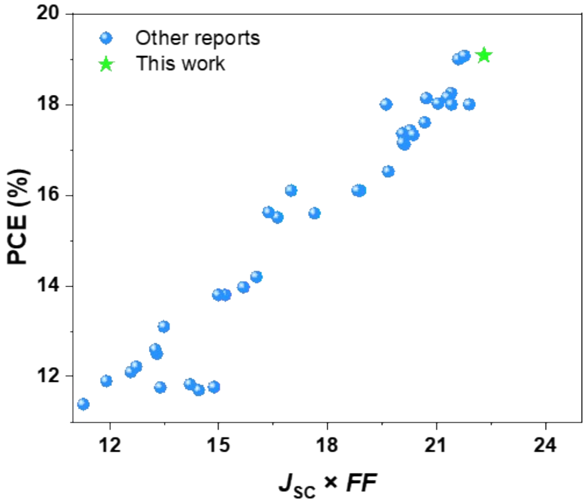

Figure S15. Efficiency comparison of non-halogenated solvent processed OSCs.

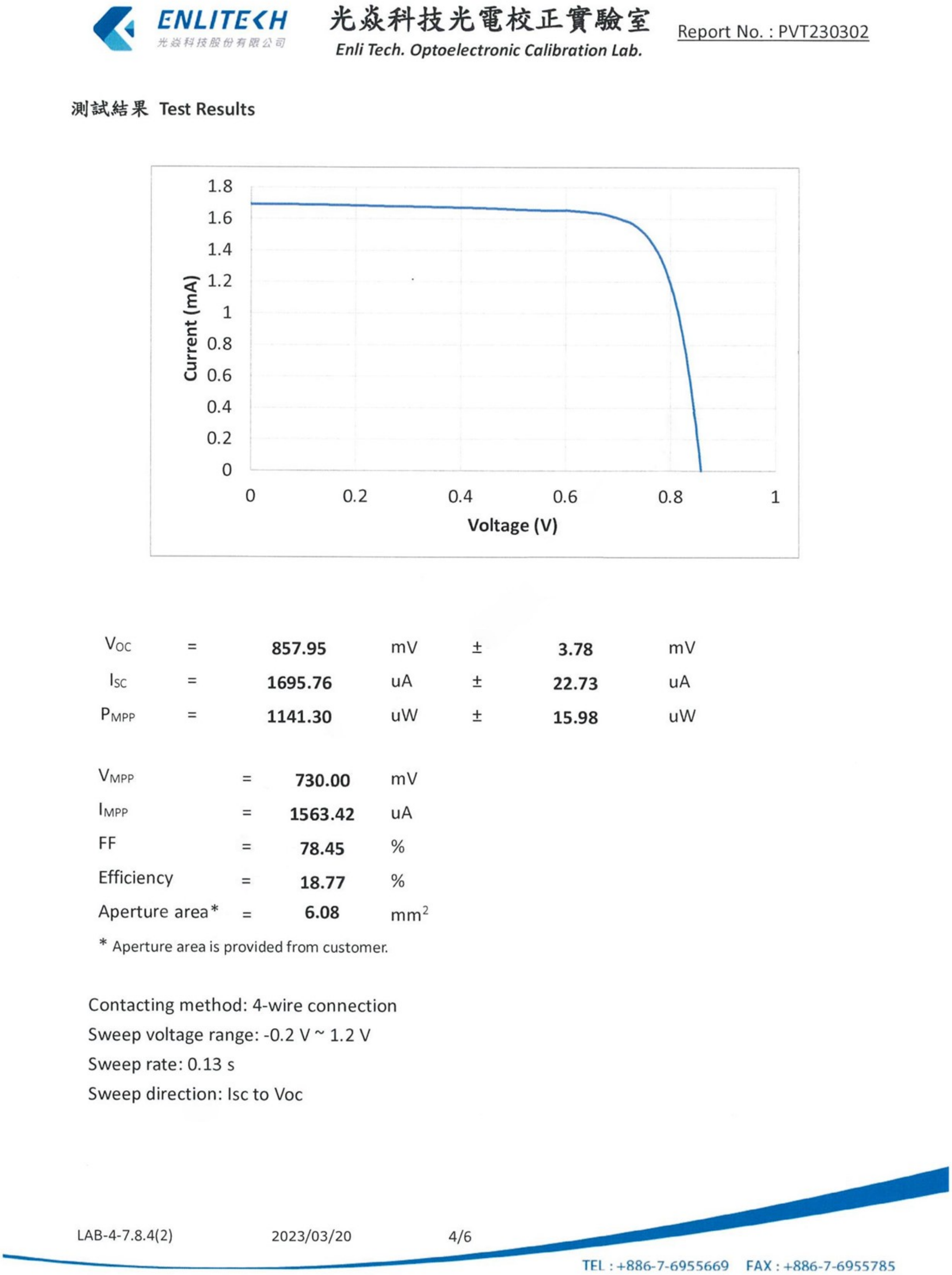

ENLITECH
光焱科技股份有限公司
光焱科技光電校正實驗室
Enli Tech. Optoelectronic Calibration Lab.
Report No. : PVT230302

測試結果 Test Results

V_{OC} = **857.95** mV ± **3.78** mV
I_{SC} = **1695.76** uA ± **22.73** uA
P_{MPP} = **1141.30** uW ± **15.98** uW

V_{MPP} = **730.00** mV
I_{MPP} = **1563.42** uA
FF = **78.45** %
Efficiency = **18.77** %
Aperture area* = **6.08** mm^2

* Aperture area is provided from customer.

Contacting method: 4-wire connection
Sweep voltage range: -0.2 V ~ 1.2 V
Sweep rate: 0.13 s
Sweep direction: Isc to Voc

LAB-4-7.8.4(2) 2023/03/20 4/6
TEL : +886-7-6955669 FAX : +886-7-6955785

Figure S16. Efficiency certification

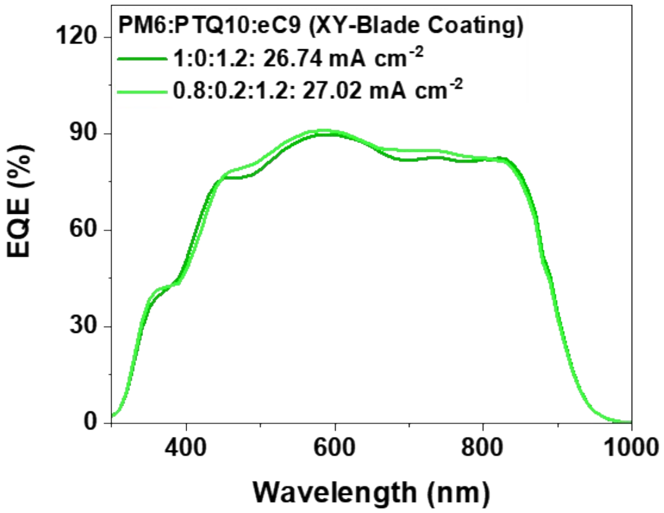

Figure S17. EQE spectra of two blade coating devices

Table S1. Device performances.

Systems	V_{OC} (V)	J_{SC} (mA cm^{-2})	*FF* (%)	PCE (%)
PM6:eC9				
CF	0.849	26.97/26.43	77.7	17.79 (17.20±0.22)
CB	0.853	26.14/25.64	78.6	17.52 (17.25±0.17)
XY	0.845	27.15/26.65	79.2	18.16 (17.60±0.24)
PM6:L8-BO				
CF	0.880	26.27/25.47	79.2	18.31 (17.80±0.33)
CB	0.860	24.39/23.96	75.3	15.79 (15.26±0.22)
XY	0.858	25.10/24.54	77.8	16.75 (16.14±0.25)

The brackets contain averages and standard errors of PCEs based on 20 devices.

Table S2. Energy loss parameters.

Systems	E_g (eV)	$EQE_{EL}@J_{SC}$	ΔE_1 (eV)	ΔE_2 (eV)	ΔE_3 (eV)	ΔE_{tot} (eV)
PM6:eC9						
CF	1.40	3.0×10^{-5}	0.25	0.03	0.27	0.55
CB	1.40	3.6×10^{-5}	0.25	0.04	0.26	0.55
XY	1.41	2.3×10^{-5}	0.25	0.04	0.28	0.57
PM6:L8-BO						
CF	1.46	5.6×10^{-5}	0.26	0.07	0.25	0.58
CB	1.45	4.1×10^{-6}	0.26	0.04	0.32	0.59
XY	1.47	5.1×10^{-6}	0.26	0.04	0.31	0.61

Table S3. Calculated parameters for (100) peak from IP direction.

Systems	Peak (Å^{-1})	d-spacing (Å)	CCL (Å)
PM6:eC9			
CF	0.31	20.94	57.7
CB	0.31	20.94	79.7
XY	0.30	20.94	58.3
PM6:L8-BO			
CF	0.31	20.94	71.6
CB	0.31	20.27	52.9
XY	0.30	20.27	51.4

Table S4. Calculated parameters for (010) peak from OOP direction.

Systems	Peak position (Å^{-1})	d-spacing (Å)	CCL (Å)
PM6:eC9			
CF	1.69	3.72	17.0
CB	1.69	3.72	18.2
XY	1.68	3.74	17.0
PM6:L8-BO			
CF	1.68	3.74	18.9
CB	1.69	3.72	18.5
XY	1.70	3.70	18.6

Table S5. Fitting for addition peaks in PM6:L8-BO film on OOP direction in lamellar region.

PM6:L8-BO	Peak (Å^{-1})	d-spacing (Å)	CCL (Å)
CB	0.49	12.82	91.2
XY	0.47	13.37	7.1

Table S6. Calculated area distribution of (100) crystallite orientation from GIWAXS data.

Systems	Edge-on area	Face-on area	Isotropic area	Edge-on percentage (%)	Face-on percentage (%)	Isotropic percentage (%)
PM6:eC9						

CF	8.70	2681.9	590.5	0.3	81.7	18.0
CB	48.1	1969.4	1094.8	1.5	63.3	35.2
XY	20.4	1869.4	1229.7	0.7	59.9	39.4
PM6:L8-BO						
CF	8.7	1432.7	829.9	0.4	63.1	36.5
CB	88.8	1500.8	2264.5	2.3	38.9	58.8
XY	87.9	1392.6	1756.9	2.7	43.0	54.3

Table S7. Photovoltaic performances of non-halogenated main solvent processed OSCs summary

Ref	**V_{OC} (V)**	**J_{SC} (mA cm^{-2})**	***FF* (%)**	**PCE (%)**
1	0.86	26.33	0.77	17.43
2	0.851	26.75	0.8	18.25
3	0.853	27.25	0.7814	18.16
4	0.879	26.7	0.809	19
5	0.85	25.76	0.781	17.12
6	0.933	22.52	0.738	15.51
7	0.947	22.78	0.746	16.1
8	0.85	25.2	0.75	16.1
9	0.84	26.9	0.796	18
10	0.91	20.5	0.74	13.8
11	0.94	19	0.7	12.5
12	0.865	26.05	0.77	17.36
13	0.856	24.94	0.755	16.1
14	0.84	26.23	0.75	16.52
15	0.96	17.97	0.7	12.1
16	0.95	18.19	0.7	12.22
17	1	18.9	0.63	11.9
18	0.92	22.47	0.667	13.8
19	0.88	17.62	0.76	11.76
20	0.784	19.8	0.73	11.7
21	0.85	26.1	0.78	17.33
22	0.95	22.1	0.741	15.62
23	0.88	24.3	0.726	15.6
24	0.89	21.1	0.76	14.2
25	0.89	23.4	0.67	13.97
26	0.97	18.74	0.72	13.1
27	0.95	18.67	0.71	12.6
28	0.83	19.2	0.74	11.83
29	0.78	20.37	0.73	11.77

30	1.01	17.89	0.63	11.39
31	0.82	28.15	0.778	18
32	0.85	26.2	0.789	17.6
33	0.856	26.535	0.793	18.02
34	0.876	27.11	0.7641	18.14
35	0.855	26.34	0.762	17.16
36	0.920	24.3	0.807	18.0
37	0.874	27.12	0.8026	19.07
This work	0.855	27.85	0.801	19.10

Reference

1. D. Wang, H. Liu, Y. Li, G. Zhou, L. Zhan, H. Zhu, X. Lu, H. Chen and C.-Z. Li, *Joule*, 2021, **5**, 945-957.

2. D. Wang, G. Zhou, Y. Li, K. Yan, L. Zhan, H. Zhu, X. Lu, H. Chen and C.-Z. Li, *Adv. Funct. Mater.*, 2022, **32**, 2107827.

3. R. Sun, T. Wang, Y. Wu, M. Zhang, Y. Ma, Z. Xiao, G. Lu, L. Ding, Q. Zheng, C. J. Brabec, Y. Li and J. Min, *Adv. Funct. Mater.*, 2021, **31**, 2106846.

4. Y. Cui, Y. Xu, H. Yao, P. Bi, L. Hong, J. Zhang, Y. Zu, T. Zhang, J. Qin, J. Ren, Z. Chen, C. He, X. Hao, Z. Wei and J. Hou, *Adv. Mater.*, 2021, **33**, 2102420.

5. H. Chen, H. Lai, Z. Chen, Y. Zhu, H. Wang, L. Han, Y. Zhang and F. He, *Angew. Chem. Int. Ed.*, 2021, **60**, 3238-3246.

6. L. Jin, R. Ma, H. Liu, W. Xu, Z. Luo, T. Liu, W. Su, Y. Li, R. Lu, X. Lu, H. Yan, B. Z. Tang and T. Yang, *ACS Applied Materials & Interfaces*, 2021, **13**, 34301-34307.

7. S. Ding, R. Ma, T. Yang, G. Zhang, J. Yin, Z. Luo, K. Chen, Z. Miao, T. Liu, H. Yan and D. Xue, *ACS Applied Materials & Interfaces*, 2021, **13**, 51078-51085.

8. L. Hong, H. Yao, Z. Wu, Y. Cui, T. Zhang, Y. Xu, R. Yu, Q. Liao, B. Gao, K. Xian, H. Y. Woo, Z. Ge and J. Hou, *Adv. Mater.*, 2019, **31**, 1903441.

9. Y. Xu, Y. Cui, H. Yao, T. Zhang, J. Zhang, L. Ma, J. Wang, Z. Wei and J. Hou, *Adv. Mater.*, 2021, **33**, 2101090.

10. C.-Y. Liao, Y. Chen, C.-C. Lee, G. Wang, N.-W. Teng, C.-H. Lee, W.-L. Li, Y.-K. Chen, C.-H. Li, H.-L. Ho, P. H.-S. Tan, B. Wang, Y.-C. Huang, R. M. Young, M. R. Wasielewski, T. J. Marks, Y.-M. Chang and A. Facchetti, *Joule*, 2020, **4**, 189-206.

11. H. Guo, Y. Zhang, L. Chen, X. Liao, Q. Xie, Y. Cui, B. Huang, C. Yang and Y. Chen, *J. Mater. Chem. A*, 2019, **7**, 27394-27402.

12. R. Ma, T. Yang, Y. Xiao, T. Liu, G. Zhang, Z. Luo, G. Li, X. Lu, H. Yan and B. Tang, *ENERGY & ENVIRONMENTAL MATERIALS*, 2022, **5**, 977-985.

13. S. Dong, T. Jia, K. Zhang, J. Jing and F. Huang, *Joule*, 2020, **4**, 2004-2016.

14. R. Sun, T. Wang, Z. Luo, Z. Hu, F. Huang, C. Yang and J. Min, *Solar RRL*, 2020, **4**, 2000156.

15. Y. Qin, L. Ye, S. Zhang, J. Zhu, B. Yang, H. Ade and J. Hou, *J. Mater. Chem. A*, 2018, **6**, 4324-4330.

16. Y. Xiong, L. Ye, A. Gadisa, Q. Zhang, J. J. Rech, W. You and H. Ade, *Adv. Funct. Mater.*, 2019, **29**, 1806262.

17. D. Liu, B. Yang, B. Jang, B. Xu, S. Zhang, C. He, H. Y. Woo and J. Hou, *Energy Environ. Sci.*, 2017, **10**, 546-551.

18. C. Zhu, Z. Li, W. Zhong, F. Peng, Z. Zeng, L. Ying, F. Huang and Y. Cao, *Chem. Commun.*, 2021, **57**, 935-938.

19. L. Zhu, M. Zhang, W. Zhong, S. Leng, G. Zhou, Y. Zou, X. Su, H. Ding, P. Gu, F. Liu and Y. Zhang, *Energy Environ. Sci.*, 2021, **14**, 4341-4357.

20. J. B. Zhao, Y. K. Li, G. F. Yang, K. Jiang, H. R. Lin, H. Ade, W. Ma and H. Yan, *Nat. Energy*, 2016, **1**, 15027.

21. X. Xu, L. Yu, H. Yan, R. Li and Q. Peng, *Energy Environ. Sci.*, 2020, **13**, 4381-4388.

22. B. Liu, H. Sun, J.-W. Lee, J. Yang, J. Wang, Y. Li, B. Li, M. Xu, Q. Liao, W. Zhang, D. Han, L. Niu, H. Meng, B. J. Kim and X. Guo, *Energy Environ. Sci.*, 2021, **14**, 4499-4507.

23. B. Du, Y. Ma, C. Guo, J. Cai, D. Li, S. Cheng, D. Liu, Q. Zheng and T. Wang, *Adv. Funct. Mater.*, 2021, **31**, 2105794.

24. Y. Cui, H. Yao, L. Hong, T. Zhang, Y. Xu, K. Xian, B. Gao, J. Qin, J. Zhang, Z. Wei and J. Hou, *Adv. Mater.*, 2019, **31**, 1808356.

25. S. J. Jeon, Y. W. Han and D. K. Moon, *Small*, 2019, **15**, 1902598.

26. W. Zhao, S. Zhang, Y. Zhang, S. Li, X. Liu, C. He, Z. Zheng and J. Hou, *Adv. Mater.*, 2018, **30**, 1704837.

27. X. Xu, T. Yu, Z. Bi, W. Ma, Y. Li and Q. Peng, *Adv. Mater.*, 2018, **30**, 1703973.

28. T. Kumari, S. Jung, Y. Cho, H.-P. Kim, J. W. Lee, J. Oh, J. Lee, S. M. Lee, M. Jeong, J. M. Baik, W. Jo and C. Yang, *Nano Energy*, 2020, **68**, 104327.

29. S. Rasool, Q. V. Hoang, D. Van Vu, T. T. Trang Bui, S.-M. Jin, T. T. Ho, C. E. Song, H. K. Lee, S. K. Lee, J.-C. Lee, S.-J. Moon, E. Lee and W. S. Shin, *J. Mater. Chem. A*, 2019, **7**, 24992-25002.

30. Y. Tang, H. Sun, Z. Wu, Y. Zhang, G. Zhang, M. Su, X. Zhou, X. Wu, W. Sun, X. Zhang, B. Liu, W. Chen, Q. Liao, H. Y. Woo and X. Guo, *Adv. Sci.*, 2019, **6**, 1901773.

31. B. Fan, F. Lin, J. Oh, H. Fu, W. Gao, Q. Fan, Z. Zhu, W. J. Li, N. Li, L. Ying, F. Huang, C. Yang and A. K. Y. Jen, *Adv. Energy Mater.*, 2021, **11**, 2101768.

32. X. Song, P. Sun, D. Sun, Y. Xu, Y. Liu and W. Zhu, *Nano Energy*, 2022, **91**, 106678.

33. R. Ma, C. Yan, P. W.-K. Fong, J. Yu, H. Liu, J. Yin, J. Huang, X. Lu, H. Yan and G. Li, *Energy Environ. Sci.*, 2022, **15**, 2479-2488.

34. H. Lu, H. Wang, G. Ran, S. Li, J. Zhang, Y. Liu, W. Zhang, X. Xu and Z. Bo, *Adv. Funct. Mater.*, 2022, **32**, 2203193.

35. Y. Li, J. Wu, H. Tang, X. Yi, Z. Liu, Q. Yang, Y. Fu, J. Liu and Z. Xie, *ACS Applied Materials & Interfaces*, 2022, **14**, 31054-31065.

36. J. Wang, Y. Cui, Y. Xu, K. Xian, P. Bi, Z. Chen, K. Zhou, L. Ma, T. Zhang, Y. Yang, Y. Zu, H. Yao, X. Hao, L. Ye and J. Hou, *Adv. Mater.*, 2022, **34**, 2205009.

37. L. Zhan, S. Yin, Y. Li, S. Li, T. Chen, R. Sun, J. Min, G. Zhou, H. Zhu, Y. Chen, J. Fang, C.-Q. Ma, X. Xia, X. Lu, H. Qiu, W. Fu and H. Chen, *Adv. Mater.*, 2022, **n/a**, 2206269.